Boxberger, T., Picozzi, M., Parolai, S. (2011): Shallow geology characterization using Rayleigh and love wave dispersion curves derived by seismic noise array measurements. - Journal of Applied Geophysics, 75, 2, 345-354

DOI: 10.1016/j.jappgeo.2011.06.032

Shallow geology characterization using Rayleigh and Love wave dispersion curves derived from seismic noise array measurements

T. Boxberger, M. Picozzi*, S. Parolai

Helmholtz Centre Potsdam GFZ German Research Centre for Geosciences, Germany

*picoz@gfz-potsdam.de

Abstract

The local geology and shallow S-wave velocity structure of a site are recognized to be key factors for the increase in the damaging potential of seismic waves. Indeed, seismic amplitudes may be amplified in frequency ranges unfavorable for building stock by the presence of soft sedimentary covers over lying hard bedrock. Hence, microzonation activities, which aim at assessing the site response as accurately as possible, have become a fundamental task for the seismic risk reduction of urbanized areas. Methods based on the measurement of seismic noise, which typically are fast, non-invasive, and low cost, have become a very attractive option in microzonation studies.

Using observations derived from seismic noise recordings collected by two-dimensional arrays of seismic stations, we present a novel joint inversion scheme for surface wave curves. In particular, the Love wave, the Rayleigh wave dispersion and the HVSR curves are innovatively combined in a joint inversion procedure carried out following a global search approach (i.e., the Genetic Algorithm).

The procedure is tested using a data set of seismic noise recordings collected at the Bevagna (Italy) test-site. The results of the novel inversion scheme are compared with the inversion scheme proposed by Parolai et al. (2005), where only Rayleigh wave dispersion and HVSR curves are used, and with a cross-hole survey.

Abbreviations:

ESAC - extended spatial autocorrelation method
GA - genetic algorithm
HVSR - horizontal-to-vertical spectral ratio
INGV-Mi - Instituto Nazionale di Geofisica e Vulcanologia - Sezione di Milano
RMS - root mean square
SPAC - spatial autocorrelation method

1. Introduction

It has been recognized for some time that the local geology is a key factor when considering the damaging potential of seismic waves. Seismic amplitudes may in fact be amplified in frequency ranges unfavorable for building stock by the presence of sedimentary covers. Hence, microzonation activities, which aim at assessing a site´s response as accurately as possible, have become a fundamental task for the seismic risk reduction of urbanized areas.

The variation of the S-wave velocity with depth and the total thickness of the sedimentary cover are the most important physical parameters controlling the amplification of seismic waves. For these reasons, during the last decades, several approaches have been developed that aim to provide in-situ measurements of S-wave velocity variations with depth. The usage of very accurate techniques such as downhole or cross-hole methods, however, are often too expensive for microzonation studies, where a large territorial coverage is mandatory. Therefore, methods based on the measurement of seismic noise, which typically are fast, non-invasive, and low cost, have become a very attractive option.

The dispersion curves of surface waves are very sensitive to S-wave velocity variations with depth (Zhang *et al*, 1996). Therefore, several approaches have been proposed in the literature to extract from seismic noise recordings information about the velocity of seismic wave propagation in the sedimentary cover. In general, all methods for retrieving surface wave dispersion curves are based on phase-coherency measurements between pairs (at least two) of signals. Aki (1957) proposed the spatial autocorrelation (SPAC) method, which recently has been generalized in the extended spatial autocorrelation (ESAC) method by Ohori et al. (2002), to extract both the Love and Rayleigh wave dispersion curves. Similarly, frequency-wavenumber approaches, including the beam-forming (BFM; Lacoss *et al*, 1969) and the maximum likelihood (MLM; Capon, 1969) methods, together with their variants, can also be successfully used for the same purpose.

Similarly, Scherbaum et al. (2003), and Arai and Tokimastu (2004) showed that Horizontal-to-Vertical Spectral Ratio (HVSR) curves from seismic noise recordings, originally proposed by Nogoshi & Igarashi

(1971), are sensitive to the shallow S-wave velocity structure of a site, and can be profitably inverted to obtain the structure.

Once the surface wave dispersion or HVSR curves of a site are available, from their inversion the S-wave velocity profile of a site can be obtained. In order to overcome the difficulties related to the non-linear nature of this inverse problem, several inversion approaches have been tested over the last few years. Among others, Parolai et al. (2006) discussed the pro and cons of both linearized and global inversion methods when applied to the inversion of Rayleigh wave dispersion curves. Scherbaum et al. (2003) showed that the independent inversions of Rayleigh wave dispersion and HVSR curves are inexorably affected by the trade-off between S-wave velocity and the thickness of the sedimentary cover. For this reason, Parolai et al. (2005) and Arai and Tokimatsu (2005) proposed the joint inversion of Rayleigh wave dispersion and HVSR curves, where in each case surface wave higher modes are included in the analysis. Similarly, Köhler et al. (2007) presented a combined inversion of Love and Rayleigh dispersion curves that takes advantage of the different sensitivity of Love and Rayleigh waves to the S-wave velocity structure.

In this work we present a joint inversion of Rayleigh and Love dispersion curves together with the HVSR curve (hereafter, LRHV inversion). This novel inversion approach is applied to seismic noise data recorded by a 2D array of seismic stations at the Bevagna (Italy) test site, where independent geological and geophysical information was available. The Rayleigh and Love dispersion curves have been estimated using the ESAC method, and specifically using the procedure proposed by Metaxian et al. (1997) for the analysis of the horizontal components of ground motion. The two dispersion curves are then combined with HVSR curves representative of the whole array into a joint inversion, based on a genetic algorithm (Parolai et al., 2005). In order to evaluate the advantages related to the proposed inversion scheme, we compared the resultant S-wave velocity profile with the one obtained by the classical joint inversion approach of Parolai et al. (2005), where only the Rayleigh dispersion and HVSR curves are considered (hereafter, RHV inversion). Moreover, we compared the inversion results with the S-wave profile obtained by a cross-hole survey made until a depth of 40 m.

Finally, both the performance of the RHV and LRHV inversion schemes and the different sensitivities of the Love, Rayleigh dispersion and HVSR curves with respect to the S-wave velocity variation with depth are discussed by comparing the resolution and Jacobian matrixes.

2. Methods

In this section we present a summary of the methods used for deriving the Rayleigh and Love waves dispersion curves, the HVSR curves, as well as the Genetic Algorithm used in the joint inversion analysis for the estimation of the S-wave velocity profile. A comprehensive literature review on the topic is reported by Foti et al. (2011).

2.1 SPatial Auto-Correlation (SPAC) and Extended Spatial Auto-Correlation (ESAC) for the vertical component of ground motion

The SPAC method was originally proposed by Aki (1957, 1965) as a statistical tool for the extraction from seismic noise of information dealing with the surface wave phase velocities in sedimentary layers. The method is based on the assumption that the seismic noise represents the sum of waves propagating without attenuation in a horizontal plane in different directions with different powers, but with the same phase velocity for a given frequency. Moreover, it is also assumed that waves with different propagation directions and different frequencies are statistically independent. As discussed in Ohori et al. (2002), when these assumption are verified, the space-correlation function for one angular frequency ω_0, normalized to the power spectrum, can be expressed in the form

$$\overline{\rho}(r,\omega_0) = J_o\left(\frac{\omega_0}{c(\omega_0)} r\right) , \qquad (1)$$

where, $c(\omega)$ is the frequency-dependent phase velocity, *r* is the interstation distance, and J_o is the zero order Bessel function. Eq. 1 provides a link between the Rayleigh wave phase velocity and the theoretical space cross-correlation function values. Considering that experimental values of the azimuthally averaged spatial correlation function $\bar{\rho}(r,\omega_0)$ can be obtained from seismic noise measurements carried out with 2D arrays of seismic stations, by fitting these latter values to the theoretical Bessel function values, the phase velocity $c(\omega)$ can be retrieved.

Typically in the SPAC method, a fixed value of r is used. However, Okada (2003) and Ohori et al. (2002) showed that, since $c(\omega)$ is a function of frequency ω, better phase-velocity estimates are achieved by fitting the spatial-correlation function at each frequency to a Bessel function, which depends on the inter-station distances (extended spatial autocorrelation, ESAC). For every pair of stations, the function $\phi(\omega)$ can be calculated in the frequency domain by means of (Malagnini et al., 1993; Ohori et al., 2002; Okada, 2003):

$$\overline{\rho}_{jn}(f) = \frac{\frac{1}{M}\sum_{l=1}^{M}\mathrm{Re}({}_{m}S_{jn}(\omega))}{\sqrt{\frac{1}{M^2}\sum_{l=1}^{M}{}_{m}S_{jj}(\omega)\sum_{l=1}^{M}{}_{m}S_{nn}(\omega)}} \quad , \qquad (2)$$

where ${}_{m}S_{jn}$ is the cross-spectrum for the mth segment of data between the jth and the nth stations and M is the total number of used segments. The power spectra of the mth segments at stations j and n are therefore expressed as ${}_{m}S_{jj}$ and ${}_{m}S_{nn}$, respectively. Hence, the experimental space-correlation values from eq. (2) are plotted for every frequency as a function of distance, and an iterative grid-search procedure can be then performed using eq. (1) in order to find the value of $c(\omega)$ that gives the best fit to the data.

2.2 ESAC for the horizontal components of ground motion

As discussed by Aki (1965), the SPAC equations derived for the analysis of the vertical component of ground motion can in principle be adapted for the analysis of the horizontal components, with the aim of extracting the phase velocities of Rayleigh and Love waves. In fact, in the case of Rayleigh waves, when they are polarized parallel to the propagation direction, equations similar to Eq. 1 can be derived for both the radial and tangential components of motion. In particular, the azimuthally averaged correlation coefficient for the radial $\overline{\rho}_r(r,\omega_0)$ and tangential $\overline{\rho}_t(r,\omega_0)$ components are expressed by

$$\overline{\rho}_r(r,\omega_0) = J_o\left(\frac{\omega_0}{c_R(\omega_0)}r\right) - J_2\left(\frac{\omega_0}{c_R(\omega_0)}r\right), \tag{3}$$

and

$$\overline{\rho}_t(r,\omega_0) = J_o\left(\frac{\omega_0}{c_R(\omega_0)}r\right) + J_2\left(\frac{\omega_0}{c_R(\omega_0)}r\right), \tag{4}$$

where J_2 is the second-order Bessel function.

Similarly, for Love waves, when they are perpendicularly polarized to the direction of propagation, $\overline{\rho}_r(r,\omega_0)$ and $\overline{\rho}_t(r,\omega_0)$ are expressed by

$$\overline{\rho}_r(r,\omega_0) = J_o\left(\frac{\omega_0}{c_L(\omega_0)}r\right) + J_2\left(\frac{\omega_0}{c_L(\omega_0)}r\right), \tag{5}$$

and

$$\overline{\rho}_t(r,\omega_0) = J_o\left(\frac{\omega_0}{c_L(\omega_0)}r\right) - J_2\left(\frac{\omega_0}{c_L(\omega_0)}r\right), \tag{6}$$

where $c_L(\omega_0)$ is the phase velocity of the Love waves.

However, during real surveys, the seismic noise in the horizontal components of ground motion is characterized by the superposition of both Rayleigh and Love waves. Thus, the extraction of phase-velocity information for the single phases is not straightforward.

For this reason, Metaxian et al. (1997) proposed, under the assumption that the contribution of both Rayleigh and Love waves is statistically independent, to adopt the equation

$$\begin{aligned}\overline{\rho}_r(r,\omega_0) = \alpha&\left[J_o\left(\frac{\omega_0}{c_R(\omega_0)}r\right) - J_2\left(\frac{\omega_0}{c_R(\omega_0)}r\right)\right]\\ +(1-\alpha)&\left[J_o\left(\frac{\omega_0}{c_L(\omega_0)}r\right) + J_2\left(\frac{\omega_0}{c_L(\omega_0)}r\right)\right]\end{aligned}, \tag{7}$$

and

$$\overline{\rho}_t(r,\omega_0) = \alpha\left[J_o\left(\frac{\omega_0}{c_R(\omega_0)}r\right) + J_2\left(\frac{\omega_0}{c_R(\omega_0)}r\right)\right] + (1-\alpha)\left[J_o\left(\frac{\omega_0}{c_L(\omega_0)}r\right) - J_2\left(\frac{\omega_0}{c_L(\omega_0)}r\right)\right], \quad (8)$$

where $\alpha(\omega)$ represents the proportion of Rayleigh and Love waves in the wave field energy . In particular, for $\alpha = 1$, the wavefield is dominated by Rayleigh waves, while for $\alpha = 0$, only Love waves exist. Eqs. (7) and (8) can therefore be exploited to retrieve Love wave phase velocity estimates. In particular, once the Rayleigh wave phase velocities are constrained by the analysis of the vertical component of motion, a similar iterative procedure can be implemented on the horizontal components of motion for the estimation of Love wave phase velocities, with only the addition of a loop accounting for the variation of the parameter α.

2.3 Horizontal-to-Vertical Spectra Ratios (HVSR)

Nakamura (1989) revised the Horizontal-to-Vertical Spectral Ratio (HVSR) technique, based on seismic noise recordings, that was first proposed by Nogoshi and Igarashi (1970, 1971). Since then, the HVSR technique has been used in site effect estimation in a large number of studies (e.g., Field and Jacob, 1993; Lermo and Chavez-Garcia, 1994; Mucciarelli, 1998; Bard, 1998; Parolai et al., 2001), especially due to its very low cost of execution. Similarly to surface wave dispersion curves, HVSR also provides information on the subsoil structure of a site. Specifically, HVSR curves are strongly conditioned by the properties (depth and S-wave velocity contrast) of the interface between the soft sediment and bedrock. Arai and Tokimatsu (2004) proposed the inversion of HVSR curves for the estimation of the S-wave velocity profile, while Parolai et al. (2005) and Arai and Tokimatsu (2005) first proposed using HVSR curves together with Rayleigh wave dispersion curves in a joint inversion scheme. Computing the HVSR corresponds to the normalization of the horizontal spectral amplitude with respect to the vertical one.

In practice, the method for evaluating HVSR curves consists of (*a*) merging the two Fourier spectra of the two horizontal components, $X(\omega)$ and $Y(\omega)$, of motion to obtain a single combined horizontal $H(\omega)$ component, whose modulus is given by

$$H(\omega) = \sqrt{(X(\omega)^2 + Y(\omega)^2)} \tag{9}$$

and (*b*) computing the ratio between these $H(\omega)$ spectra with the one from the vertical component.

2.4 Genetic Algorithm (GA) Inversion

As discussed before, both the surface wave dispersion and HVSR curves provide the necessary information for S-wave velocity estimation. However, the relationship between the surface wave velocities and HVSR curves and the S-wave velocity and sediment thickness is not linear.

Until only a few years ago, most works dealing with estimating the S-wave velocity profile of a site using seismic noise recordings focused only on the separate inversion of either the Rayleigh wave dispersion curve or the HVSR curves. However, as shown by Scherbaum et al. (2003), the HVSR ratio and the Rayleigh wave dispersion curve display different sensitivities to the S-wave velocity and thickness of the sedimentary layers. In particular, they showed that when these curves are inverted singularly, there is an un-resolvable trade-off between the model parameters that hampers the analysis results. Therefore, to overcome this drawback and the non-linear nature of the inverse problem, Parolai et al. (2005) proposed a joint inversion of Rayleigh wave phase velocity and HVSR curves using a genetic algorithm (*GA*) while also considering also the higher modes. They showed that with this approach, the trade-off between the model parameters can be reduced and a reliable evaluation of the local S-wave velocity structure can be obtained. In fact, the dispersion curve provides a constraint on the S-wave velocity of the soft sediments, while the fundamental frequency, f_0 estimated from the *HVSR* ratio peak, represents a constraint for the total sedimentary-cover thickness.

Parolai et al. (2005) proposed to perform the joint inversion of the Rayleigh wave dispersion and HVSR curves using the genetic algorithm (GA) code presented by Yamanaka and Ishida (1996). Indeed, GAs (Goldberg, 1989) belong to the class of evolutionary algorithms that generate solutions for the optimization of non-linear inverse problems by the analysis of thousands of possible models and by the usage of techniques inspired by the natural evolution theory of Darwin, such as inheritance, mutation, selection and crossover.

Parolai et al. (2005) showed the efficiency of joint inversion strategies in generating models near the global optimal solution (i.e., shear-wave velocity models able to justify both the observed Rayleigh wave dispersion and HVSR curves) using a cost function defined as

$$\text{cost} = \left[(1-p)N + pK\right]\left\{\frac{1-p}{N}\left[\sum_{j=1}^{N}\left(\frac{c_{R_o}(f)-c(f)}{c_{R_o}(f)}\right)^2\right] + \frac{p}{K}\left[\sum_{j=1}^{K}\left(\frac{hv_o(f)-c(f)}{hv_o(f)}\right)^2\right]\right\}, \quad (10)$$

where the subscript *o* indicates the observed data, and N, and K are the number of data points for the Rayleigh wave dispersion and HVSR curves, respectively.

In this study, we slightly modified the Eq. (10) in order to include within the joint inversion scheme the Love wave dispersion curve. Hence, a new cost function was defined as

$$\text{cost} = \left[(1-p-q)N + qM + pK\right]\left\{\frac{1-p-q}{N}\left[\sum_{j=1}^{N}\left(\frac{c_{R_o}(f)-c_R(f)}{c_{R_o}(f)}\right)^2\right] + \frac{q}{M}\left[\sum_{j=1}^{M}\left(\frac{c_{L_o}(f)-c_L(f)}{c_{L_o}(f)}\right)^2\right] + \frac{p}{K}\left[\sum_{j=1}^{K}\left(\frac{hv_o(f)-hv(f)}{hv_o(f)}\right)^2\right]\right\}, \quad (11)$$

where M is the number of points in the Love wave dispersion curve. The relative influence of the data sets in Eqs. (10) and (11) is controlled by the parameters p and q, where p controls the relative importance of the HVSR curve and q of the Love wave dispersion curve. That is to say, if p or q are set equal to zero, then the HVSR or Love wave dispersion curves are not considered during the inversion.

Finally, the forward modeling of Rayleigh and Love wave phase velocities and of HVSR curves was performed using an improved Thomson-Haskell method proposed by Wang (1999). This included the influence of higher modes of surface waves in both the dispersion and HVSR curves following the equations proposed by Tokimatsu et al. (1992) and Arai and Tokimatsu (2004), under the assumption of vertically heterogeneous 1D earth models.

3 The Bevagna test site

3.1 Data acquisition

In September 2007, an array of 15 seismic stations was installed in the village of Bevagna (Italy) by INGV-MI near the BVG accelerometric station of the Italian Accelerometric Network. The same data set has been used by Puglia et al. (2011) for a study of site effects, based on the separate inversion of Rayleigh and Love wave dispersion curves. All stations were equipped with Lennartz LE-3D/5s three component sensors using a Reftek 130 digitizer. Figure (1) shows the selected array geometry, which is characterized by side lengths of 170 and 85 m, and a minimum inter-station distance of 10 m. The selected range of station inter-distances allows for an optimal compromise between resolution at shallow depths and the maximum depth of investigation. Seismic noise was recorded at 500 Hz sampling rate for over 3 hours. Moreover, cross-hole measurements of the S-wave velocity down to 40 m depth have been carried out within the framework of the DPC-INGV S6 project in 2006 (Deliverable, 2009), making the shallow structure of the site quite well constrained.

3.2 ESAC on vertical and horizontal components

The Rayleigh wave phase velocities were computed by analyzing the seismic noise recorded on the vertical component, using 300 windows of signal of 30 seconds length. In order to reduce leakage problems, each signal window was tapered for 5 per cent of its length using a cosine function.

Figure (2) shows an example of the application of the ESAC analysis for 4 frequencies. The space-correlation values for every frequency are plotted as a function of distance, and an iterative grid-search procedure was performed using Eq. (1) in order to find the Rayleigh phase velocity value that gives the best fit to the observed data. The tentative phase velocity was generally varied over large intervals (e.g., between 100 and 3000 m/s) in small steps (i.e., 1 m/s). The best fit is achieved by minimizing the root mean square (RMS) of the differences between the values calculated using Eqs. (1) and (2). Following Parolai et al., (2006), three grid-search iterations were performed, and data points, which differ by more than two standard deviations from the value obtained with the minimum-misfit velocity, were removed before the next iteration. Then, using the Rayleigh wave phase velocities constrained so far, the procedure detailed in section 2.2 was performed using the horizontal components of the seismic noise ground motion to estimate the Love wave dispersion curve. With respect to the analysis carried out on the vertical component, Eqs. (7) and (8) were used, and only an additional loop was added to the iterative procedure to take into account variations of the parameter α (i.e., between 0 and 1 with steps of 0.1), which measures the proportion of Rayleigh and Love waves within the seismic noise (Metaxian et al. 1997). The number of seismic noise windows considered, the window length, and the phase velocity range used in the grid search procedure were the same as for vertical component.

Figure (3) shows the contour plot of the RMS values derived using Eqs. (7) and (8) and the experimental spatial correlation coefficients when α is varied between 0 and 1 for each frequency. Interestingly, a rather stable trend in the proportion of Rayleigh and Love waves within the seismic noise wavefield is observed in the frequency range 1.5 to 2.5 Hz, where Rayleigh and Love waves constitute about 30% and 70% of the seismic noise, respectively. However, we observed that the proportion of Rayleigh wave content increases with increasing frequency, until a value of between 70- 90 % at 4 Hz. Figure (4) shows the results of the ESAC procedure when applied to the horizontal component of ground motion for the same frequencies as in Figure (2). In this case, the minima observed in the different RMS functions indicates the phase velocity of Love waves.

Finally, Figure (5) shows for the frequency range 1.3 Hz to about 5 Hz the comparison between the Rayleigh and Love wave dispersion curves together with the associated uncertainties. Unfortunately, outside of this frequency range, it was not possible to obtain reliable estimates of the phase velocity. The two dispersion curves show a similar trend for the frequency range 3.4 to 5 Hz, which corresponds to the shallower portion of the subsurface. By contrast, for frequencies below 3 Hz, the two dispersion curves diverge considerably.

3.3 HVSR

The HVSR were computed for all the stations of the array, again using 300 windows of 30 seconds length, tapered with a cosine function for 5 per cent of their length. Figure (6) shows that most of the stations are characterized by a predominant peak at 1.3 Hz with amplitudes of around 6. Only for three stations located in the northern part of the array (BE01, BE09, and BE13) does the 1.3 Hz peak display a broader shape, probably due to the presence of spurious signals generated by a nearby small road and an irrigation canal.

Some of the HVSR curves (e.g., BE01, BE03, BE07, and BE15 in Figure 6) showed a further secondary peak at frequency around 0.3-0.4 Hz. Unfortunately, most of the stations show for frequencies below 0.5 Hz an anomalous increasing trend in the HVSR curve, probably due to tilt effects affecting the horizontal components of the sensors (Forbriger, 2006). Therefore, in order to avoid introducing to the inversion analysis observations that might be biased by systematic errors, we decided to neglect the HVSR peak at frequency between 0.3-0.4 Hz. Moreover, we selected the HVSR from station BE14 (Figure 4, subplot), as being representative of the majority of the curves to be included in the joint inversion scheme, since it shows a clear peak at 1.3 Hz, but is not affected by any artificial trend in the lower frequencies.

3.4 Inversion analysis

In this section we present the S-wave velocity results obtained by the inversion analyses. Following the procedure described in section 2.4, we first show the RHV inversion results and then compare them to those obtained by the LRHV inversion scheme.

3.4.1 Joint inversion of Rayleigh wave dispersion and HVSR curves (RHV)

As discussed in the previous section, the inversion based on GA does not employ any explicit starting models, but requires suitable parameter limits for each layer of the model to be defined. In this case, we inverted for the parameters S-wave velocity (V_S) and thickness (H), which as shown by Arai and Tokimatsu (2004) are the parameters that most influence the propagation of surface waves into the ground. Therefore, during the inversion analysis, the thickness and S-wave velocity of each layer could vary within pre-defined ranges, while the density (d) and the P-wave velocity (V_P) were constrained. In particular, the density was set by selecting values from the literature in agreement with *a priori* geological information, while the V_P were related to the S-wave velocity using the relationship of Kitsunezaki *et al*. (1990) $V_P = 1.1 \cdot V_S + 1290$, where both V_S and V_P are expressed in m/s.

Different parameterizations of the model were tested, and finally we selected one consisting of 4 layers. In order to avoid over-parameterization, the range of thicknesses explored by the GA were increased with depth. In table (1) the tested parameter ranges of the S-wave velocity and layer thicknesses are presented.

The GA inversion consisted of 150 generations of a population of 50 models. Moreover, the inversion was repeated starting from 5 different seed numbers, i.e., from a different population of initial models, with the aim of increasing the exploration of the model parameters space and thus increasing the probability of converging towards the global minimum of the inverse problem.

Following Parolai et al. (2005), within the cost function (Eq. 13) we weighted the two data-sets using a value of 0.9 for the Rayleigh wave dispersion curves and 0.1 for the HVSR curves. The inversion was performed over the frequency band 1.25-5.3 Hz for the Rayleigh wave dispersion curves and 0.5-5.3 Hz for the HVSR curves.

Figure (7) shows the results of the GA inversion procedure. The best-fit S-wave velocity profile is characterized by a significant impedance contrast at about 16 m depth, and by a second deeper impedance contrast at about 85 meters. Using the best-fit S-wave velocity profile, and computing the average velocity ($\overline{V_S}$) at the different impedance contrasts, we estimated the theoretical fundamental resonance frequency for SH-waves [i.e., $f_0 = \frac{\overline{V_S}}{4H}$] for the different layers. Interestingly, we found that a value of f_o comparable to the maximum in the HVSR curve is found for the impedance contrast at 16m of depth. On the contrary, for the impedance contrast at 85 m, a value of f_o around 0.6 Hz is found. In light of these observations, the HVSR and Rayleigh wave dispersion curves cooperate in constraining the impedance contrast at 16 m, while the deeper contrast is constrained only by the Rayleigh waves phase velocity.

The misfit function (Figure 7b) of the seed number leading to the best fit model shows a consistent decreasing trend during the first 20 generations, and then a rather stable trend with continuously decreasing misfit with increasing numbers of generations. It worth noting that the theoretical Rayleigh wave dispersion and HVSR curves computed for the best-fit model are in good agreement with the observed curves, and lay inside their uncertainty bounds. These observations suggest that the GA found a solution close to the global minimum of the inverse problem.

The distribution of the family of models with misfits within 10% RMS of the best-fit model (hereafter, models-10%) around the best-fit model itself is a further indication of the quality of the solution. Focusing on this feature within Figure (7a), we observe that for the 1st and 3rd layers, the models-10% are very close to the best-fit model, indicating that these two layers are well constrained. On the other hand, for the 2nd and 4th layers, the models-10% display that a range of other possible V_S and H values could justify, in terms of the chosen misfit functions, in a very similar way the observations. Therefore, despite the very good quality of the inversion results, it seems that the Rayleigh wave dispersion and the HVSR curves are not able to constrain with the same robustness the different portions of the model. This is consistent with previous studies (see among the others Scherbaum et al., 2003; Köhler et al. 2007), that showed the different sensitivities of HVSR, Rayleigh wave and Love wave dispersion curves to the S-wave velocity profile of the site. For this reason, in order to improve our estimates of the S-wave velocity profiles from seismic noise recordings, in a further test we also included the Love wave dispersion curves within the joint inversion scheme.

3.4.2 Joint inversion of Love and Rayleigh wave dispersion and HVSR curves (LRHV)

The joint inversion of Love and Rayleigh wave dispersion and HVSR curves was carried out following the same strategy described in section 3.4.1. That is to say, the same number of layers and range of values for the model parameters, the same number of generations and seed numbers, as well as the same information in terms of Rayleigh wave dispersion and HVSR curves were used. The only differences we introduced into this new inversion scheme were the inclusion of the Love wave dispersion curve shown in Figure (5) and the use of the new cost function expressed by Eq. (14). In particular, after tests carried out on synthetic data sets, we selected the weights p and q of Eq. (14) to equal 0.1 and 0.3, respectively, as the optimal values for combining the information given by the different curves during the inversion, that is to say to obtain an optimal fit of all the data sets used in the inversion.

Figure (8) shows the results of the novel GA joint inversion. Interestingly, despite the best-fit model of the LRHV inversion showing general characteristics very similar to those of the best-fit model from the RHV inversion, it presents some important new features. In fact, the velocity variation between the 1st and 2nd layer of the model hints at an inversion of the S-wave velocity with depth (Figure 8a). Moreover, we observe that in the present inversion results, especially in the range 15-25m depth, the LRHV models-10% are less dispersed around the best-fit model than the RHV ones (Figure 7). Furthermore, the LRHV results appear to better constrain the depth and value of the main impedance contrasts at around 18 and 95m depth.

Also for the LRHV analysis, the misfit values reached a stable minimum plateau with the increasing generation number (Figure 8b), suggesting that no improvement can be expected by continuing the process and that the final solution is likely to lie in the vicinity of the global minimum of the inversion problem. Moreover, Figures (8b and c) show that the best-fit model allows us to reproduce very well the trends in all three experimental curves.

3.5 Quantitative comparison of the RHV and LRHV results

The results presented in Figure (8) already suggested qualitatively that including the Love wave dispersion curves together with the Rayleigh wave dispersion and HVSR curves within a joint inversion scheme allows us to better constrain the S-wave velocity profile. However, in order to quantify the improvement in the solution, the inversion results are also compared using different criteria.

The first one is based on calculating for the two best-fit models of the LRHV and RHV inversions the model resolution matrices (Menke, 1989) while considering the experimental derived surface wave dispersion and HVSR curves. Although the problem is non-linear, we expect that the obtained final models will lie close to the global minimum of the solution. Picozzi and Albarello (2007) showed that in such cases, a linear inversion can be carried out to refine the velocity models. Here, we only take advantage of the linearization of the problem to study how the procedure and data can be reliably constrained through the analysis of the model and data resolution matrices. In fact, focusing on the diagonal elements of the resolution matrixes, which represent how much each of the model parameters is resolved by the experimental observations, Figure (9) shows that including the Love wave dispersion curves improves the resolution of the first two layers of the model. The reason for the improvements in the results from the LRHV inversion can be understood by analysing the Jacobian matrixes in Figure (10). Each Jacobian matrix is defined as the matrix of the first-order partial derivative, here numerically calculated, of one of the observations (Love wave dispersion, Rayleigh wave dispersion, or HVSR) with respect to the model parameters (in this case, the S-wave velocity at different depth). The distribution of maxima within the Jacobian matrix in Figure (10) indicates for which change in velocity at depth is each frequency of the Rayleigh, Love wave dispersion and HVSR curves more sensitive.

The comparison of Figures (10a and b) shows that in the frequency range 2 Hz to 5 Hz, Love waves are much more sensitive to the very shallow material properties (i.e., less than 10 m), while Rayleigh waves have a higher sensitivity at a depth of around 10 m. For frequencies less than 2 Hz, both Love and Rayleigh waves tend to be sensitive to the model characteristics over the depth range 20 m to 50 m. Finally, the HVSR curve shows for frequencies around the peak at about 1.3 Hz a high sensitivity to the model characteristics at a depth of around 20 m, which corresponds to the impedance contrast between the 2nd and 3rd layers in Figure (8a). These observations confirm that the main HVSR peak is constrained by the impedance contrast between these layers, while the second deeper impedance contrast at around 90 m is constrained by the surface wave dispersion curves. The evidence of different sensitivities with respect to different model parameters explains well why the joint inversion performed including all the surface wave derived curves, that is to say Love, Rayleigh wave dispersion and HVSR curves, can provide a better constrained S-wave velocity model.

Figure (11) shows the comparison of both the best-fit models and models-10% with the S-wave velocity profile obtained by cross-hole (CH) measurements. In general, both the best-fit S-wave velocity profiles RHV and LRHV are in good agreement with the S-wave CH profile. However, interestingly, this comparison confirmed that by including the Love wave dispersion curve in the inversion scheme (Figure 11b) the S-wave velocities in the shallow layers can be better retrieved, as well as the S-wave velocity increase at about 16 m depth. Moreover, as also observed in Figure (8), when the Love wave dispersion curve is included in the analysis, the models-10% are considerably closer to the relevant best-fit model, indicating a higher capacity of the inversion scheme to constrain the optimal solution.

4 Conclusion

In this work we introduce a joint inversion of Love wave dispersion, Rayleigh wave dispersion and HVSR curves using a data set of seismic noise recordings collected by a 2D array of seismic stations at the Bevagna (Italy) test-site.

In the first part of the work, we summarized the methods used for the estimation of the different surface wave derived curves, as well as for their inversion. In particular, we focused on the estimation of the Love wave dispersion curve using the ESAC approach on the horizontal component of the seismic noise ground motion.

In the second part of the work, we focused on the joint inversion analysis of the observed surface wave curves. In particular, we performed the inversion of real data using the joint inversion scheme proposed by Parolai et al. (2005), where only Rayleigh wave dispersion and HVSR are included, and by novel joint inversion scheme where the Love wave dispersion curves are also included. The comparison of the results from the two inversion analyses highlights that including the Love wave dispersion curves allows for the shallower portion of the S-wave velocity model to be better resolved. This point is confirmed by several observations. For example, when the joint inversion includes the Love wave dispersion curve, the family of models with misfit values close to the best-fit model of the inversion (i.e., the minimum plus the 10%) are distributed within a very narrow domain around the best-fit model itself, indicating that the solution of the inverse problem is very well constrained. Moreover, comparing the resolution matrixes for the final best fit models obtained by the RHV and LRHV schemes showed that when Love waves are considered, the shallower layers of the model can be better resolved. Finally, comparing the S-wave velocity models estimated following the two approaches with a-priori information from a cross-hole survey confirmed that the joint inversion of Love wave dispersion, Rayleigh wave dispersion, and HVSR curves can help to better constrain the S-wave velocity soil structure.

In fact, the Jacobian matrixes estimated with respect to the different observations clearly show how each of the inverted surface wave curves has a high sensitivity to a specific range of model parameters. In particular, Love waves provide more information about the shallower parts of the model, the Rayleigh waves allow the investigation of a deeper portion of the S-wave velocity profile, while the HVSR peak constrains the main impedance contrast. In conclusion, the three surface wave related curves appear to complement each other very well, and we believe that their joint inversion within the framework of microzonation studies potentially allows a more detailed characterization of the subsoil structure.

Acknowledgments:

We would like to thank Editor-in-chief K. Holliger D. Albarello and one anonymous reviewer for their comments and suggestions that allowed us to significantly improve the manuscript.

The data set used in this work is part of the INGV-DPC S4 Research Project "Italian Strong Motion Data Base", promoted by the Istituto Nazionale di Geofisica e Vulcanologia (INGV) and funded by the Dipartimento della Protezione Civile (DPC) of the Italian Government (Agreement INGV-DPC 2007-2009). The authors wish to thank the DPC and the project team coordinators, Dr. Francesca Pacor and Prof. Roberto Paolucci, and Dr. R. Puglia for provided the data set. The INGV-Mi team (composed of Dr. Dino Bindi, Ezio D'Alema, Sara Lovati and Dr. Marco Massa) who previously executed the in situ microtremor measurements is also warmly acknowledged. K Fleming kindly improved the English.

REFERENCES

Aki, K. (1957). Space and time spectra of stationary stochastic waves, with special reference to microtremors. Bulletin of the Earthquake Research Institute 35, 415–456.

Aki, K. (1965). A note on the use of microseisms in determining the shallow structures of the earth's crust. Geophysics 29, 665–666.

Arai, H. and K. Tokimatsu (2004). S-wave velocity profiling by inversion of microtremor h/v spectrum. Bulletin of the Seismological Society of America 94, 53–63.

Arai, H. and K. Tokimatsu (2005). S-wave velocity profiling by joint inversion of microtremor dispersion curve and horizontal-to-vertical (h/v) spectrum. Bulletin of the Seismological Society of America 95, 1766–1778.

Bard, P. Y. (1998). Microtremor measurement: a tool for site effect estimation? Second International Symposium on the Effects of the Surface Geology on Seismic Motion ESG98, Japan.

Capon, J. (1969). High-resolution frequency-wavenumber spectrum analysis. Proceedings of the IEEE 57(8), 1408–1418.

Chávez-Garcia, F. J. and J. Lermo (1994). Are microtremors useful in site response evaluation? Bulletin of the Seismological Society of America 84, No. 5, pp. 1350-1364

Deliverable, (2009). Responsibles: Pacor, F. Paolucci, R.; edited by: Foti, S., Parolai, S. Albarello, D.; contributors: Albarello, D., Comina, C., Foti, S., Maraschini, M., Parolai, S., Picozzi, M., Puglia, R. Tokeshi, K. Technical report, of DPC-INGV S4 Project 2007-2009.

Field, E. H., and K. Jacob (1993). The theoretical response of sedimentary layers to ambient seismic noise, Geophysical Research Letters . 20–24, 2925–2928.

Forbriger, T. (2006). Low frequency limit for H/V studies due to tilt, Arbeitgruppe-Seismology Session, 4–6 October, Haidhof.

Foti, S. Parolai, D. Albarello, and M. Picozzi (2011). Application of surface-wave methods for seismic site characterization. 2011, *Surv Geophys*. DOI 10.1007/s10712-011-9134-2.
Goldberg, D.E. (1989) .Genetic Algorithms in Search, Optimization and Machine Learning, Addison-Wesley, Reading, MA.

Kitsunezaki, C., N. Goto, Y. Kobayashi, T. Ikawa , M. Horike, T. Saito, T. Kurota, K. Yamane and K. Okuzumi (1990). Estimation of P- and S- wave velocities in deep soil deposits for evaluating ground vibrations in earthquake. J. JSNDS,9, 1-17.

Köhler, A., M. Ohrnberger, F. Scherbaum, M. Wathelet, and C. Cornou (2007). Assessing the reliability of the modified three-component spatial autocorrelation technique. Geophysical Journal International . 168, 779–796

Lacoss, R., E. Kelly, and M. Toksöz (1969). Estimation of seismic noise structure using arrays. Geophysics 34, 21–38.

Malagnini, L., A. Rovelli, S. Hough, and L. Seeber (1993). Site amplification estimates in the garigliano valley, central italy, based on dense array measurements of ambient noise. Bulletin of the Seismological Society of America 83, 1744–1755.

Menke, W., (1989). Geophysical data analysis: Discrete inverse theory, Academic Press, ISBN 0-12-490921-3.

Metaxian, J.-P., P. Leesa, and J. Dorel (1997). Permanent tremor of masaya volcano, nicaragua:Wave field analysis and source location. Journal of Geophysical Research 102,NO. B10, 529–545.66

Mucciarelli, M. (1998). Reliability and applicability of Nakamura's technique using microtremors: an experimental approach, Journal of Earthquake Engineering. 2, 625-638.

Nakamura, Y. (1989). A method for dynamic characteristics estimations of subsurface using microtremors on the ground surface. Q. Rept. RTRI Jpn. 30, 25–33.

Nogoshi, M. and T. Igarashi (1971). On the amplitude characteristics of microtremor (part2).Journal Seism. Soc. Jpn. 24, 26–40.

Ohori, M., A. Nobata, and K. Wakamatsu (2002). A comparison of esac and fk methods of estimating phase velocity using arbitrarily shaped microtremor arrays. Bulletin of the Seismological Society of America 92(6), 2323–2332.

Okada, H. (2003). The Microtremor Survey Method. Geophysical monograph series 12.

Parolai, S., P. Bormann, and C. Milkereit. (2001). Assessment of the natural frequency of the sedimentary cover in the Cologne area (Germany) using noise measurements, Journal of Earthquake Engineering. **5,** 541–564.

Parolai, S., M. Picozzi, S. M. Richwalski, and C. Milkereit (2005). Joint inversion of phase velocity dispersion and h/v ratio curves from seismic noise recordings using a genetic algorithm, considering higher modes. Geophysical Research Letters 32, L01303.

Parolai, S., S. M. Richwalski, C. Milkereit, and D. Fäh (2006). S-wave velocity profiles for earthquake engineering purposes for the cologne area (germany). Bulletin of Earthquake Engineering 4, 65–94.

Picozzi, M., and D. Albarello (2007). Combining Genetic and Linearized algorithms for a two-step joint inversion of Rayleigh wave dispersion and *H/V* spectral ratio curves. *Geophysical Journal International Vol. 169 Issue 1 Page 189 April 2007*

Puglia R., K. Tokeshi, M. Picozzi, E. D'Alema, S. Parolai, S. Foti (2011).Interpretation of microtremor 2D array data using Rayleigh and Love waves: the case study of Bevagna (central Italy). Submitted to Near Surface Geophysics

Scherbaum, F., K.-G. Hinzen, and M. Ohrnberger (2003). Determination of shallow shearwave velocity profiles in cologne, germany area using ambient vibrations. Geophysical Journal International 152, 597–612.

Tokimatsu, K., S. Tamura, and H. Kojima (1992). Effects of multiple modes on Rayleigh wave dispersion characteristics. Journal of Geotechnical Engineering 118, 1529–1543.

Wang, R. (1999). A simple orthonormalization method for stable and efficient computation of Green's functions. Bulletin of the Seismological Society of America. 89 733–41

Yamanaka, H. and H. Ishida (1996). Application of generic algorithms to an inversion of surface-wave dispersion data. Bulletin of Earthquake Engineering 86, 436–444.

Zhang B, M Yu, Lan C Q and Xiong W 1996 Elastic waves and excitation mechanism of surface waves in multilayered media J. Acoust. Soc. Am. 100 3527–38

Tables

	thickness[m]		v_S [m/s]	
layer	min	max	min	max
1	5.00	20.00	70.00	230.00
2	5.00	20.00	100.00	300.00
3	30.00	80.00	200.00	600.00
4	10.00	40.00	250.00	650.00

Table 1: Parameter range of depth [m] and S-wave velocity [m/s] for the joint inversion of the Bevagna measurement considering 4 different layers

FIGURES

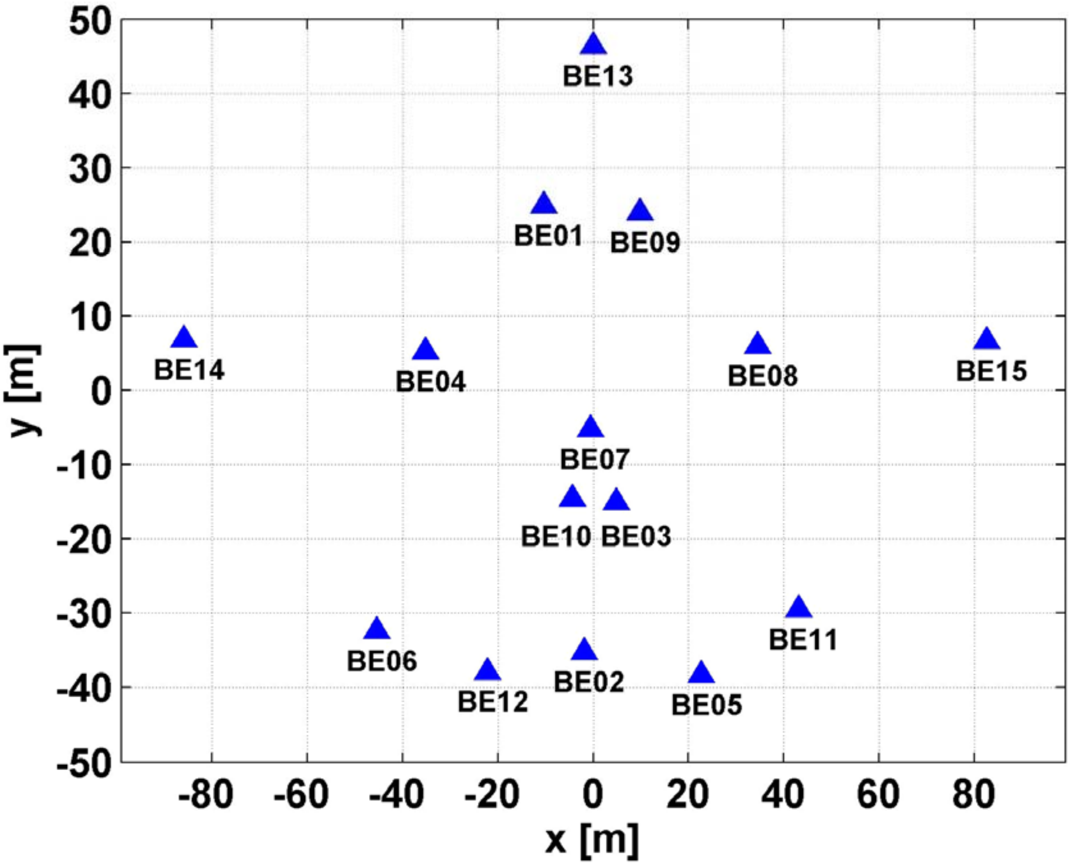

Figure 1: Array geometry of the Bevagna test site measurement.

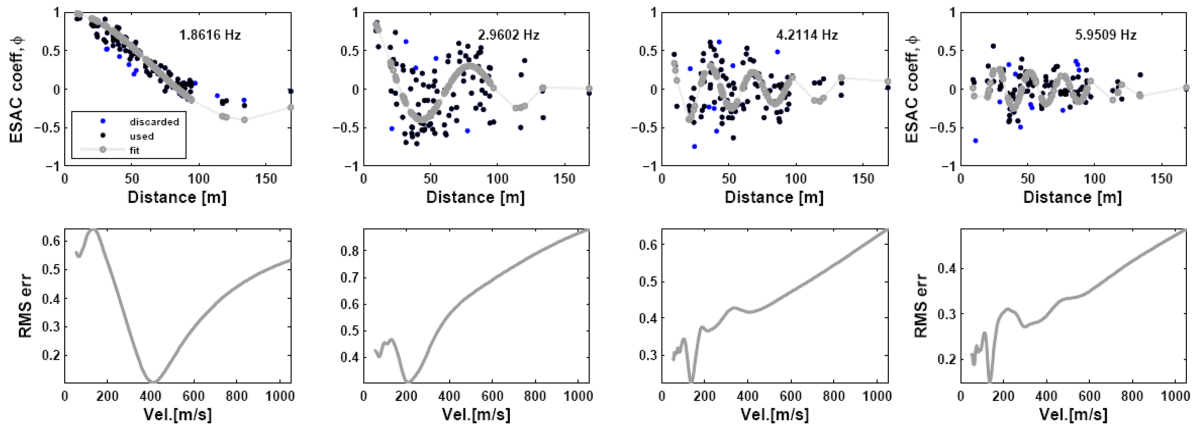

Figure 2: Top row: ESAC function values (black circles) for different frequencies and the vertical component. The blue circles indicate the discarded values. The grey lines depict the best-fitting Bessel function. Bottom row: RMS error versus phase velocity curves.

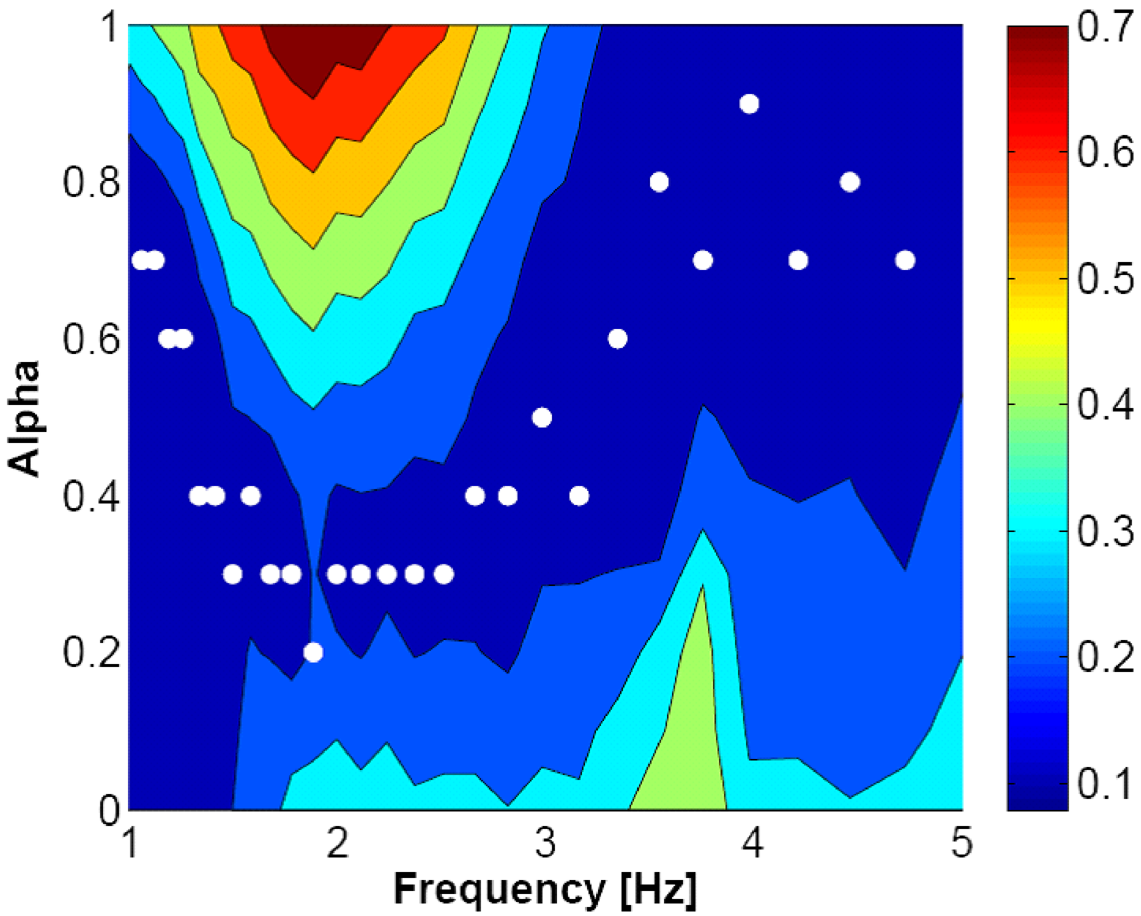

Figure 3: Distribution of α values (white dots) for different frequencies and the associated RMS error.

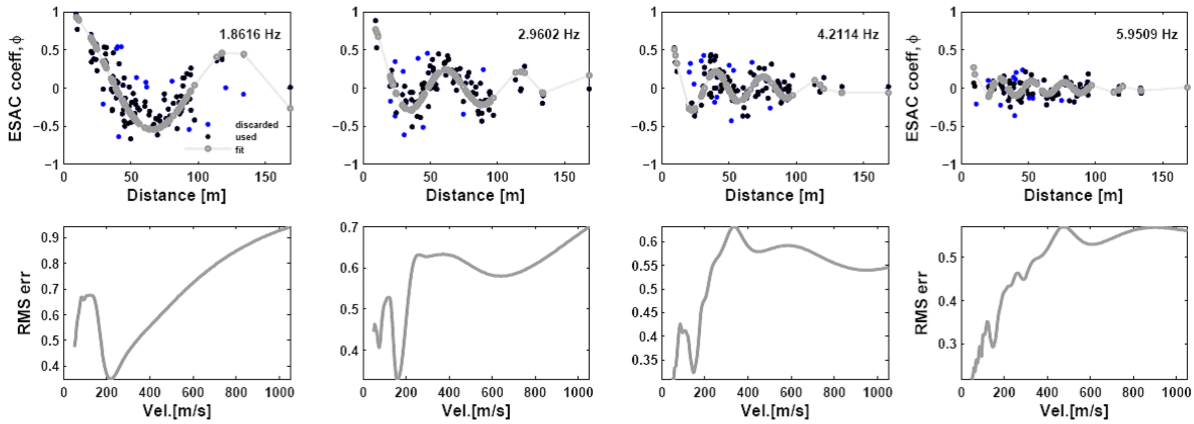

Figure 4: Top row: ESAC function values (black circles) for different frequencies and the horizontal components. The blue circles indicate the discarded values. The grey lines depict the best-fitting Bessel function. Bottom row: RMS error versus phase velocity curves.

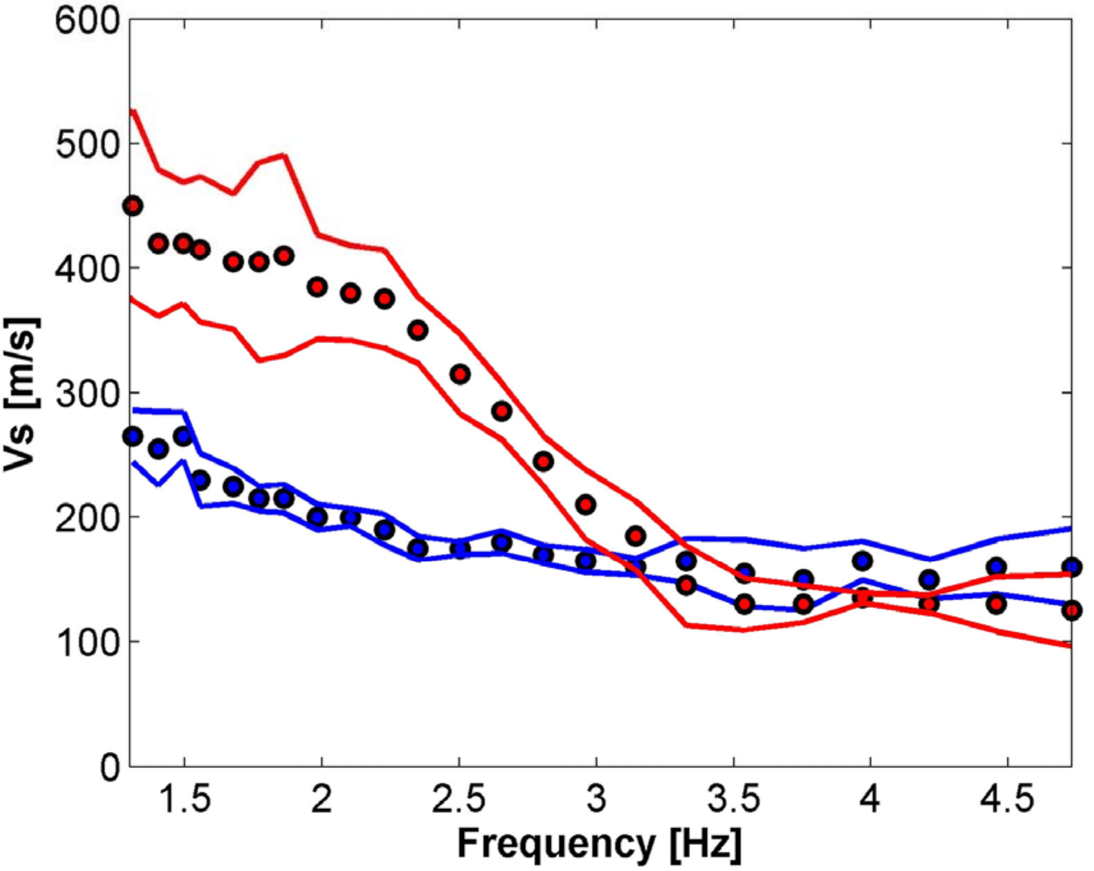

Figure 5: Rayleigh (red) and Love (blue) wave dispersion curves.

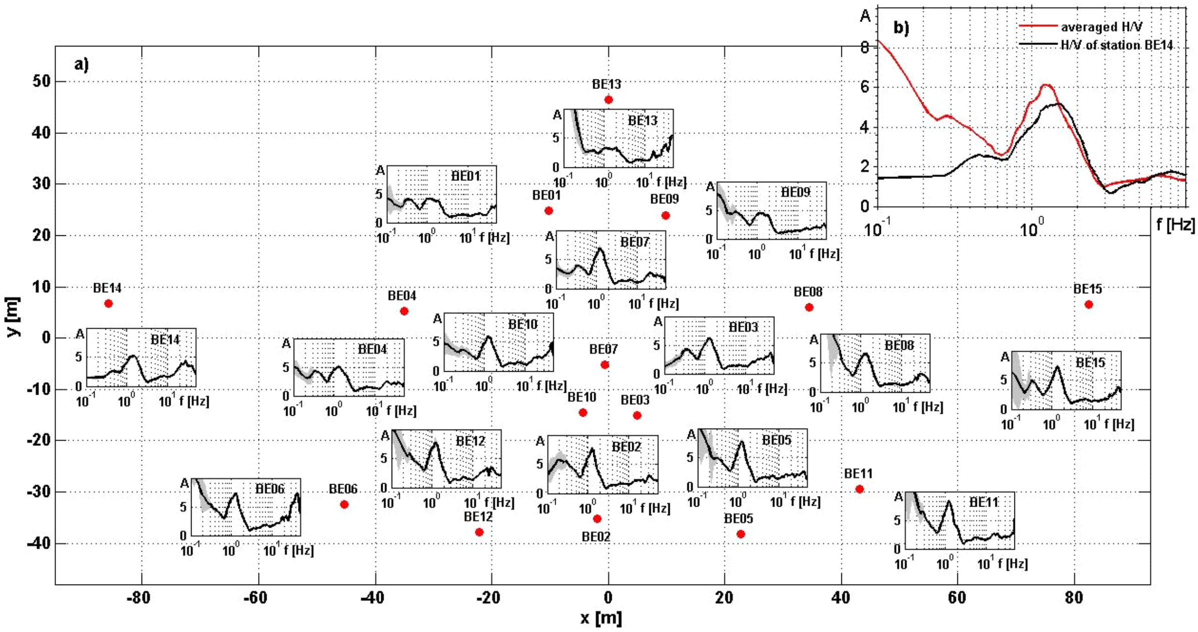

Figure 6: H/V spectral ratio curves of the array microtremor measurements from Bevagna. a) H/V curves of all stations together with their positions. b) H/V curve of station BE14 compared with the averaged H/V curve of all stations.

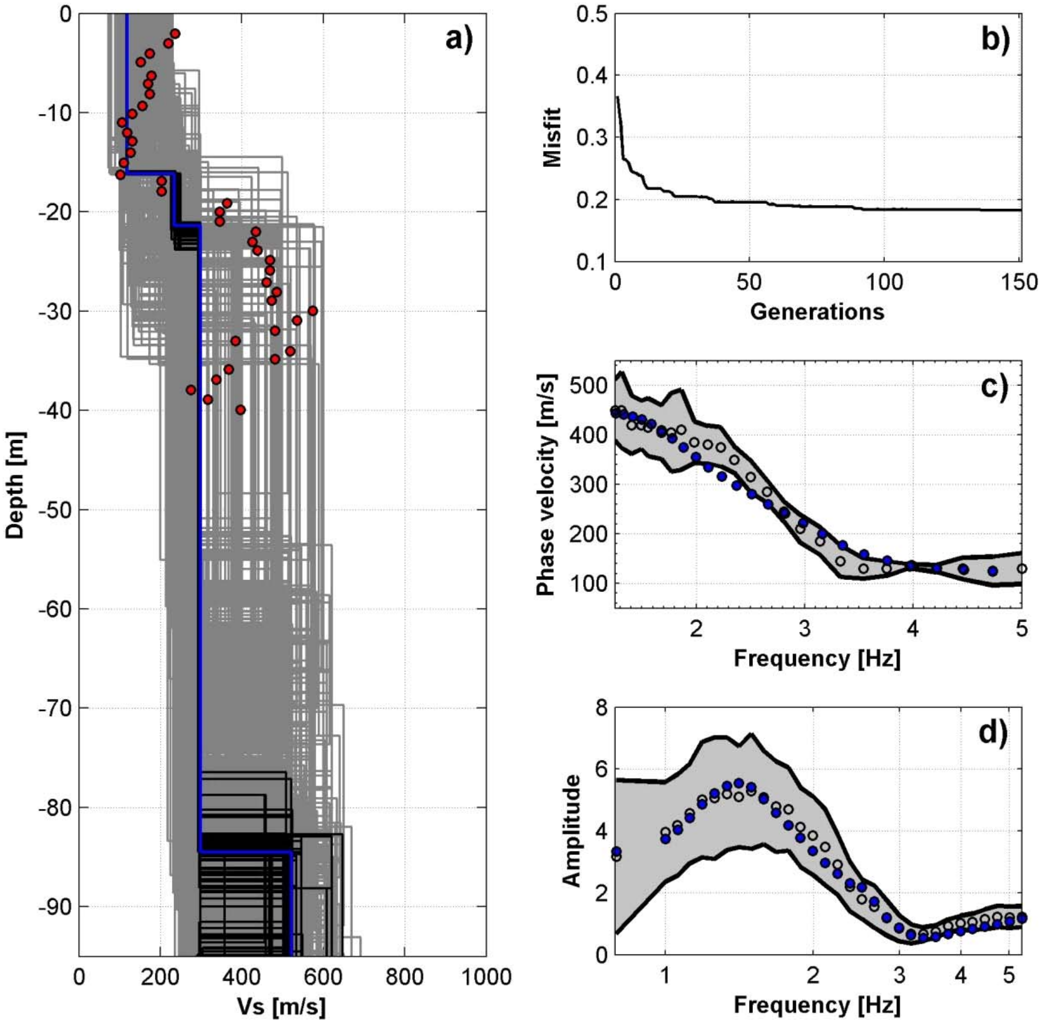

Figure 7: a) S-wave velocity profile from the RHV joint inversion; best fit model (blue line), models in a range of the best fit model + 10 % (black lines), all models (gray lines) b) misfit for all 150 generations c) observed (open circles) and calculated (blue circles) Rayleigh wave dispersion curve, standard deviation values (grey lines) of the observed dispersion curve d) observed (open circles) and calculated (blue circles) H/V spectral ratio, standard deviation values (grey lines) of the observed H/V curve.

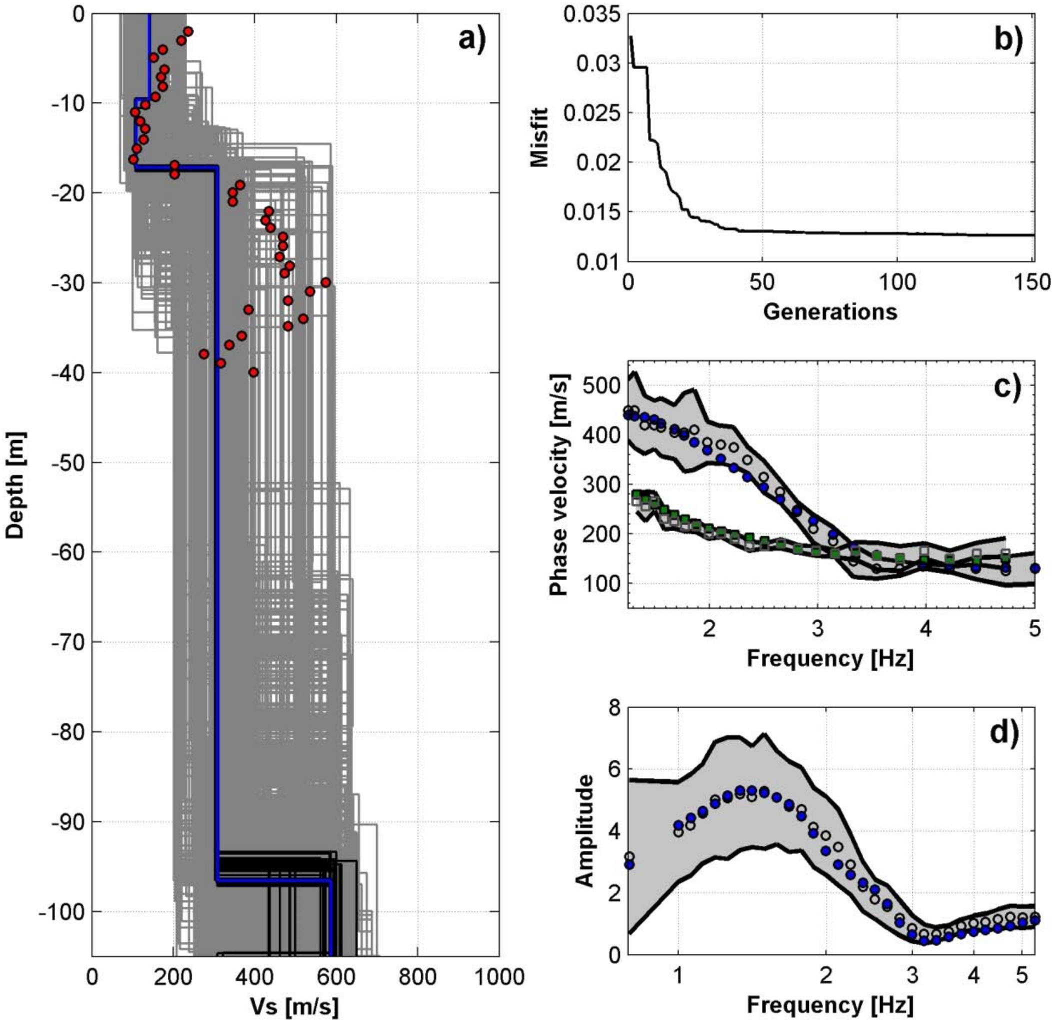

Figure 8: see Figure 7; additional c) observed (gray squares) and calculated (green squares) Love wave dispersion curve.

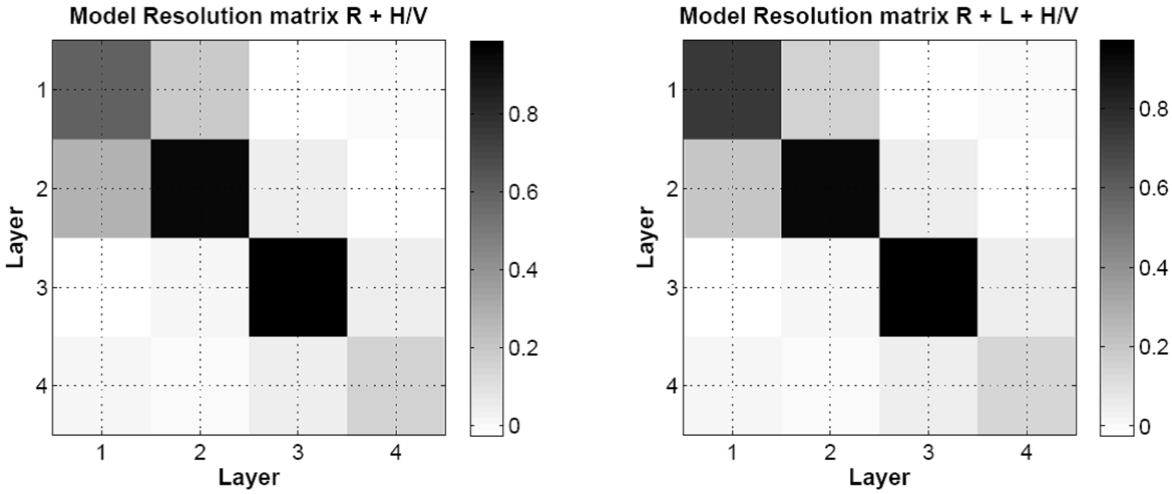

Figure 9: Model resolution matrices: left) RHV inversion, right) RLHV inversion.

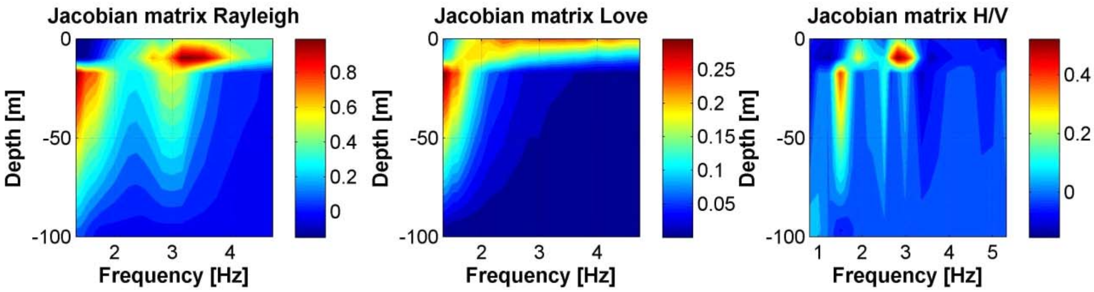

Figure 10: Jacobian matrix for Rayleigh and Love wave dispersion curve and H/V curve.

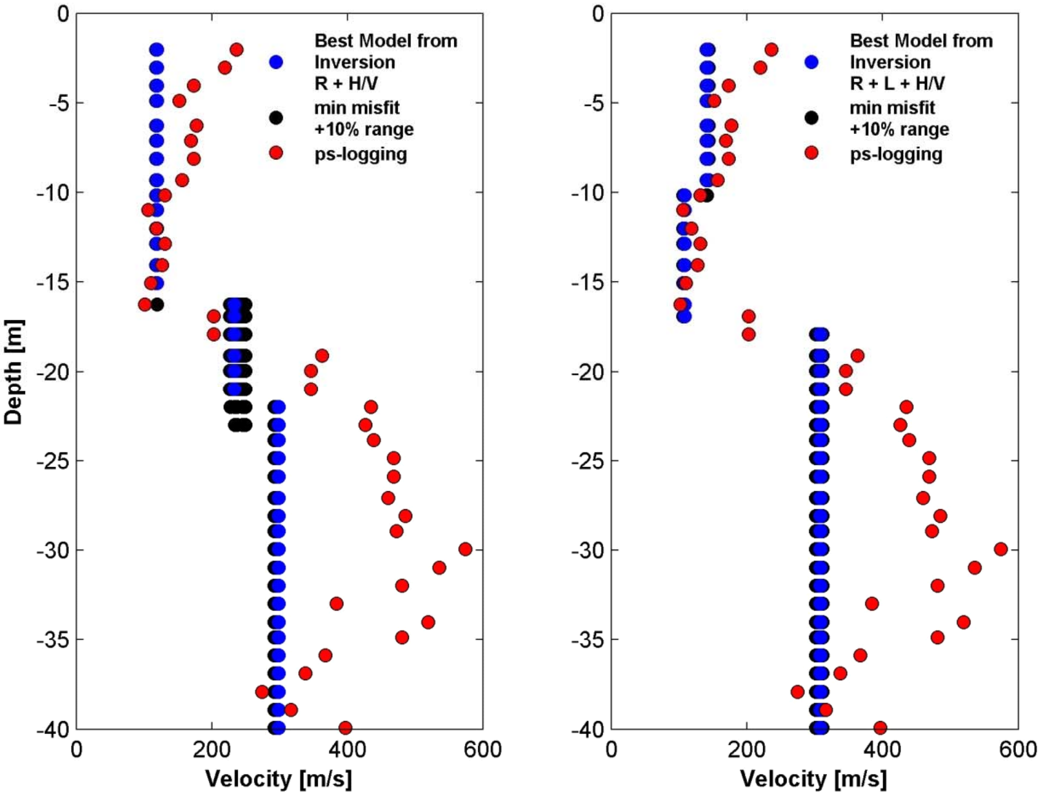

Figure 11: Best fit models and models in a range of 10% of the best fit model in comparison to CH data for RHV (left) and RLHV (right) inversion.